Available online at www.sciencedirect.com
ScienceDirect
Catalysis Today 120 (2007) 203–213
CATALYSIS TODAY
www.elsevier.com/locate/cattod

Flame sprayed visible light-active Fe-TiO_2 for photomineralisation of oxalic acid

Wey Yang Teoh [a], Rose Amal [a,*], Lutz Mädler [b], Sotiris E. Pratsinis [c]

[a] *ARC Centre for Functional Nanomaterials, School of Chemical Engineering and Industrial Chemistry, The University of New South Wales, Sydney, NSW 2052, Australia*

[b] *Department of Chemical and Biomolecular Engineering, University of California, Los Angeles, 405 Hilgard Avenue, Los Angeles, CA 90095, USA*

[c] *Particle Technology Laboratory, Institute of Process Engineering, Department of Mechanical and Process Engineering, Swiss Federal Institute of Technology (ETH) Zürich, CH-8092 Zürich, Switzerland*

Available online 24 August 2006

Abstract

Visible light-active Fe-doped TiO_2 was prepared by a one-step flame spray pyrolysis (FSP) technique. The properties of the photocatalysts were characterised by UV–vis diffuse-reflectance spectroscopy, X-ray diffraction (XRD), X-ray photoelectron spectroscopy (XPS), nitrogen adsorption (BET), transmission electron microscope (TEM) and zeta potential techniques. Being a bottom-up approach, the short residence time coupled with rapid quenching during FSP resulted in homogeneous Fe-doped TiO_2 for Fe/Ti ratios approximately up to 0.05. This is five times higher than that reported for particles synthesised by conventional wet techniques followed by high temperature annealing. Under visible light irradiation ($\lambda > 400$ nm), the rate of oxalic acid mineralisation by Fe-doped TiO_2 (Fe/Ti = 0.05) was 6.4 times higher than that of similarly prepared bare TiO_2 and Degussa P25. A unique Fe-leaching and re-adsorption properties were observed during the reaction. Unlike the system of bare TiO_2 spiked with dissolved Fe(III) ions, the FSP Fe-doped TiO_2 photocatalyst was found to be stable and reusable after each run with minimal loss of Fe from the surface.

Keywords: Flame spray pyrolysis; Photocatalysis; Visible; Solid solution; Oxalic acid

1. Introduction

The landmark report by Fujishima and Honda [1] on water splitting using a single rutile crystal has triggered tremendous interests in the field of TiO_2 photocatalysis, even after more than three decades. Many innovative TiO_2 photocatalysis applications have arisen from their work, which include organics syntheses [2], solar cell [3], cancer therapy [4], water and air purifications [5], cathodic corrosion protection [6], anti-fogging glass [7] and self-cleaning materials [8]. However, TiO_2 particles can only be activated by high energy wavelength ($\lambda < 400$ nm) and thus only make use of approximately 4% of the solar spectrum that reaches the earth surface.

In view of this, many researchers have attempted to modify the relatively large bandgap energy of TiO_2 (3.2 eV) so that it can be activated by visible light irradiation ($\lambda > 400$ nm). Dyes adsorbed and/or supported on semiconductors to give visible light responsive catalysts [3,9] have been extensively investigated. However the dye compounds lack thermal and photochemical stability. A separate approach is to dope the semiconductor with small amount of cations and/or metal oxides by wet chemical impregnation [10,11]. Although in principle the introduction of cations into TiO_2 by wet syntheses is capable of inducing visible light sensitisation, they exist mostly as impurities and promote charge recombination. Hence no noticeable enhancement in photocatalytic activity could be observed for these catalysts under visible light illumination [12,13]. Studies have shown that high energy implantation of metal cations (V, Cr, Fe, Co and Ni) into the TiO_2 matrix [13–15] resulted in photocatalytic characteristics under visible light, with 25–32% solar light absorption. Visible light sensitive TiO_2 films can also be prepared using a similar concept but by employing radio frequency magnetron sputtering [16]. Furthermore, the introduction of Groups IV–VI atoms, in

* Corresponding author. Tel.: +61 2 9385 4361; fax: +61 2 9385 5966.
E-mail address: r.amal@unsw.edu.au (R. Amal).

0920-5861/$ – see front matter © 2006 Elsevier B.V. All rights reserved.
doi:10.1016/j.cattod.2006.07.049

particular nitrogen [17–19], sulphur [20–22] and carbon [23–25] into TiO_2 matrix has also been reported to sensitise TiO_2 in the visible light range.

Although substitutional doping of TiO_2 with Fe could extend its photoresponse to visible light range [10,11,15,26–28], mixed photocatalytic activity results were obtained. Yamashita et al. [15] found significant improvement in the degradation of aqueous 2-propanol by Fe ion implanted TiO_2 under visible light illumination. Li et al. [26] reported enhancement in the oxidation of cyclohexane to cyclohexanol by sol–gel prepared Fe-TiO_2, also under visible light irradiation. However, Nagaveni et al. [27] found detrimental effect of Fe-TiO_2 prepared by solution combustion for the degradation of 4-chlorophenol under solar radiation. Likewise, Reddy et al. [29] observed detrimental effect in the visible light degradation of 4-chlorophenol using TiO_2-loaded Fe/MCM-41 prepared by hydrothermal method. In general, there is still a large discrepancy in the literature between reactivity of visible light photocatalysts prepared using different techniques and the target organic compounds.

In this work, Fe-doped TiO_2 photocatalysts are synthesised using a flame spray pyrolysis (FSP) technique [30,31]. Being a bottom-up approach, the gas-to-particle synthesis coupled with rapid quenching during FSP facilitates the synthesis of homogeneously doped materials. The photocatalysts of different Fe content are specifically evaluated for visible light photocatalytic activity. Oxalic acid is chosen as the model organic compound for the photocatalytic oxidation studies due to its molecular simplicity and being a frequently found pollutant in textile, pharmaceutical, metallurgy and nuclear wastewater [32,33]. It is also a commonly encountered degradation intermediate of many complex organic pollutants.

2. Experimental

2.1. Photocatalyst synthesis by flame spray pyrolysis

The liquid precursor used to synthesise bare TiO_2 was similar to that previously described elsewhere [34,35]. It consisted of a mixture of titanium isopropoxide (TTIP, Aldrich, purity >97%)/xylene (Riedel deHaen, 96%)/acetonitrile (Fluka, 99.5%), in the volume ratio of 20/55/25. Both the xylene and acetonitrile reagents were dried with molecular sieve (10–20 mest beads, Fluka) prior to use. A predetermined amount of iron naphthenate (12% Fe in mineral spirits, Strem) was added to the precursor mixture. During FSP [31], a flow of 5 mL/min of liquid precursor was delivered to the nozzle using a syringe pump (Inotech R232). The precursor was then atomised by 5 L/min of dispersant O_2 while maintaining a pressure drop of 1.5 bar at the nozzle tip. Combustion of the dispersed droplets by the surrounding supporting methane/oxygen (1.5 L/min/3.2 L/min) forms the main core flame. Additional 5 L/min sheath O_2 was issued through the outer most sintered metal ring. All gases used were sought from BOC Gases (Australia). The photocatalyst was collected on a glass fibre filter (Whatmann GF/D, 25.7 cm diameter) using a vacuum pump (Alcatel SD Series).

2.2. Photocatalyst characterisation

UV–vis diffuse-reflectance spectroscopy was used to characterise the optical absorption properties of bare and Fe-doped TiO_2 photocatalysts. The diffuse-reflectance spectra of the dry powders were measured using a Varian Cary 5 UV–vis-NIR spectrophotometer equipped with an integrating sphere. To study the absorption properties of the used photocatalysts, the illuminated suspension was centrifuged (Beckmann-Coulter Allegra 25R Centrifuge) at 10 000 rpm for 20 min followed by vacuum drying. The bandgap energies of the doped TiO_2 were estimated assuming indirect semiconductor [36]. The bandgap energy was estimated by the straight-line intercept fitted to a graph of $[F(R) \times h\nu]^{1/2}$ versus $h\nu$, where $F(R)$ is the Kubelka–Munk function as measured by UV–vis and $h\nu$ is the energy of the incident photon.

Crystal morphology of the photocatalysts was studied using X-ray diffraction (XRD) analysis on Philips XRD 1140 operating at 30 kV, 30 mA (Co Kα and Co Kβ radiation). The powder was scanned at 2θ from 20 to 70°, 0.01° per step and 5 s per step. Crystallite phase identification was carried out using PANalytical X'Pert Highscore Plus software. To determine crystallite size and composition, Cu Kα was used as the radiation source scanning at 2θ from 22° to 32°, 0.02° per step and 5 s per step. Scherrer equation was used to determine the crystallite sizes of anatase and rutile without considering the effect of microstrain. The composition of rutile was determined from the following equation as described by Spurr and Myer [37]:

$$\chi_{\text{rutile}} = \left(1 + \frac{0.8 I_{\text{A}}}{I_{\text{R}}}\right)^{-1} \quad (1)$$

where χ_{rutile} is the weight fraction of rutile and I_{A} ($2\theta = 25.4°$) and I_{R} ($2\theta = 27.6°$) are the XRD peak intensities of anatase (1 0 1) and rutile (1 1 0), respectively.

The specific surface area (SSA) of the photocatalyst samples was measured using Micromeritics Tristar 3000 by means of nitrogen adsorption at 77 K, using the BET (Brunauer–Emmett–Teller) method. Prior to analysis, the photocatalysts were degassed under vacuum at 150 °C for 1.5 h. A full 40-point adsorption–desorption isotherm was performed on the powder samples. Powder samples were suspended in methanol and sonicated before being dispersed onto carbon-coated copper grids. The particle-loaded grids were studied under Philips CM200 Transmission Electron Microscope operating at 200 kV. Surface elemental composition and Fe oxidation states of Fe-doped TiO_2 particles before and after 5 runs of photocatalytic oxidation of oxalic acid were characterised using X-ray Photoelectron Spectroscopy on ESCALab220i-XL (VG Scientific). A monochromated Al Kα (20 eV pass energy) the pressure chamber was evacuated to $<2 \times 10^{-9}$ mbar.

Photocatalyst suspension (1 g/L) was extracted during photocatalytic reaction to monitor the particle zeta potential dynamics. The suspended particle zeta potential was measured by means of electrophoretic mobility on a Brookhaven ZetaPals system. To study the extent of Fe-leaching from the photocatalysts, the change in dissolved Fe concentration during

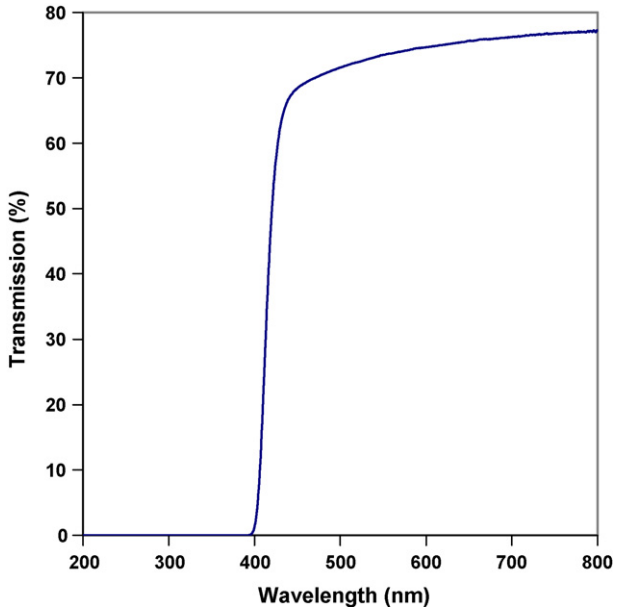

Fig. 1. UV–vis transmission profile for a double layer of Rosco® E-colour UV filter.

photocatalytic reaction was measured by Varian Inductively Coupled Plasma–Atomic Absorption Spectroscopy (ICP–AAS). The photocatalyst suspension was passed through a PTFE membrane syringe filter (0.2 μm, Sartorius) to recover approximately 5 mL of the filtrate for analysis.

2.3. Photocatalyst evaluation

Photocatalyst suspension of 1 g/L was circulated in a 200 mL closed system slurry-type spiral photoreactor [38]. The set-up allows for monitoring of CO_2 evolution based on conductivity measurements (Jenway 4330) as described by Abdullah et al. [38]. The suspension was prepared using deionised water (Millipore) and sonicated for approximately 15 min. Diluted perchloric acid was added to adjust the suspension pH to 3.25 ± 0.25. Prior to testing, a carbon burnoff step was carried out by irradiating the suspension with UVA lamp (NEC T10 blacklight blue, 20 W) to remove any organic impurities on the photocatalyst surface. This step was carried out until no further increase in conductivity reading was recorded. The suspension was air-equilibrated before injecting oxalic acid (Unilab, anhydrous) (equivalent to 2000 μm carbon or 10 ppm carbon) and mixed for a further 20 min in the dark. Photocatalytic reaction was initiated by illuminating the suspension with a fluorescent lamp (Davis 33 cool white, 18 W) filtered with a double layer of Rosco® E-colour UV filter to remove any UV component ($\lambda < 400$ nm) (see Fig. 1).

3. Results and discussion

3.1. Photoresponse and bandgap energy of bare and Fe-doped TiO_2

Both Degussa P25 and FSP-made TiO_2 particles do not exhibit any absorption in the visible regime as shown in the

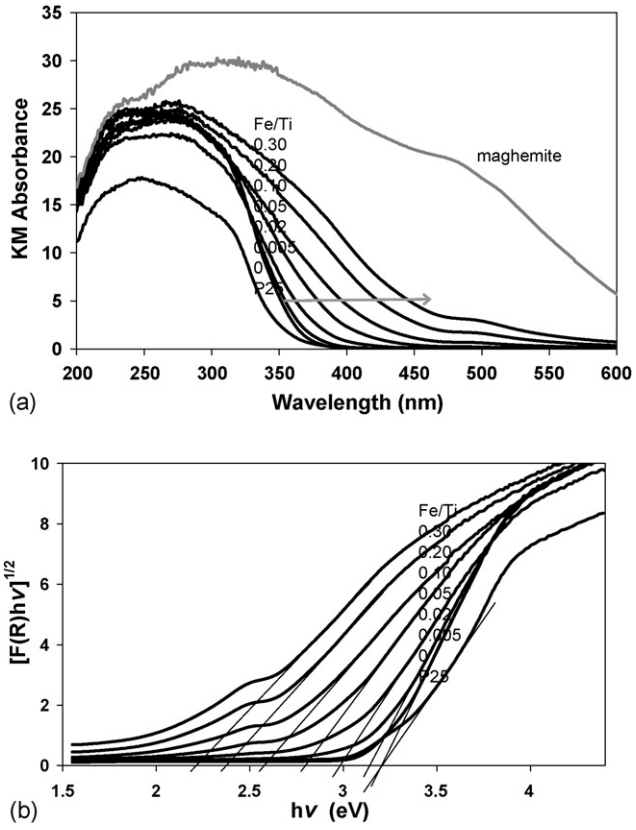

Fig. 2. (a) UV–vis Kubelka–Munk absorption $F(R)$ of as-prepared pure and Fe-doped TiO_2 photocatalysts and (b) the modified Kubelka–Munk plots of the same samples for their optical bandgap energies estimation.

Kubelka–Munk (KM) absorption plot (Fig. 2a). The absorption threshold for both TiO_2 samples was approximately 388 nm, equivalent to an optical bandgap energy (E_g) of 3.20 eV. This value was obtained from the modified KM absorption plot (Fig. 2b). The similarity in bandgap energy for the two TiO_2 samples is expected as both have similar crystallite phase composition, consisting predominantly of anatase (∼80%, E_g = 3.20 eV) and the rest rutile (E_g = 3.02 eV) [34,35].

Increasing the Fe-dopant content in FSP-TiO_2 shifts the photocatalyst response to higher wavelengths (Fig. 2a and b). As the Fe/Ti ratio is increased from 0.005 to 0.30, the absorption threshold of doped TiO_2 is gradually increased from 396 to 564 nm, corresponding to bandgap energies of 3.13 to 2.20 eV, respectively.

Doping Fe cations into TiO_2 lattice results in the formation of impurity energy level (IEL) between the conduction and valence band of TiO_2 [11,27,39]. This IEL allows for intrinsic bandgap excitation such that under illumination of visible light, the higher energy state of 3d-electrons from Fe-dopant (relative to the ground state electrons of TiO_2) could be excited to the TiO_2 conduction. Using the *ab initio* band calculation based on density function theory (DFT) with the full-potential linearised-augmented-plane-wave (F-LAPW) method, Umebayashi et al. [39] found the position of Fe-dopant IEL to be close to the TiO_2 valence band. They suggested that the electrons are localised around the dopant ions. This further supports the postulation that electrons could in fact be excited from the IEL.

It is interesting to note the existence of an absorption band centred at ~490 nm for Fe-doped TiO_2 with Fe/Ti ratios ≥0.10 (Fig. 2a). The existence of this optical absorption band remains unclear. Nagaveni et al. [27] also observed similar absorption band for Fe-TiO_2 prepared by solution combustion. They attributed the band to the d–d transition of Fe-dopant. Using low temperature (0 °C) hydrolysis without further annealing, Serpone et al. [11] reported a similar band but centred at ~470 nm for colloidal Fe-TiO_2 particles. The band was again suggested to arise from the d–d transition of Fe. Navío et al. [40] and Li et al. [26] reported absorption band that was centrally shifted to 530 nm in Fe-TiO_2 synthesised by wet impregnation and sol–gel methods, respectively, followed by calcination at high temperature. However they attributed this to the formation of segregated hematite as confirmed by XRD. Although hematite is the thermodynamically stable phase at high temperature, the high quenching rate during FSP yielded a metastable, maghemite-like phase. Fig. 2a shows that the absorption band of this FSP-made maghemite is centred at ~470 nm, not 490 nm, ruling out the possibility of maghemite formation in the FSP Fe-doped TiO_2. The absence of this segregated phase was further confirmed using XRD phase identification (Section 3.2). The absorption band remains even after leaching with 0.1N of H_2SO_4 for 48 h (Fig. 3). Likewise, the bandgap energies of all Fe-doped TiO_2 were only slightly affected after acid treatment, indicating stability of the Fe-dopant.

3.2. Crystallographic properties of pure and Fe-doped TiO_2

Substitution of Ti^{4+} (0.61 Å, hexacoordination) by Fe^{3+} (0.55 Å, hexacoordination) [41] into the TiO_2 lattice is highly feasible during the bottom-up FSP synthesis given the similarity in their ionic radii. No Fe segregation or formation of a new crystallite phase could be observed from the XRD spectra (Fig. 4). All the XRD peaks corresponded well with anatase and rutile phases, for Fe/Ti ≤ 0.05. It is believed that the short residence time coupled with high quenching rate [42] during the flame synthesis prevents phase segregation once Fe^{3+} is incorporated into Ti^{4+}. It can be seen from Figs. 4 and 5 that increasing Fe loading greatly promotes the formation of rutile. This is consistent with Al-doping of TiO_2 in hot-wall [43] or vapour-fed flame reactors [44] with Al^{3+} (0.53 Å) substituting

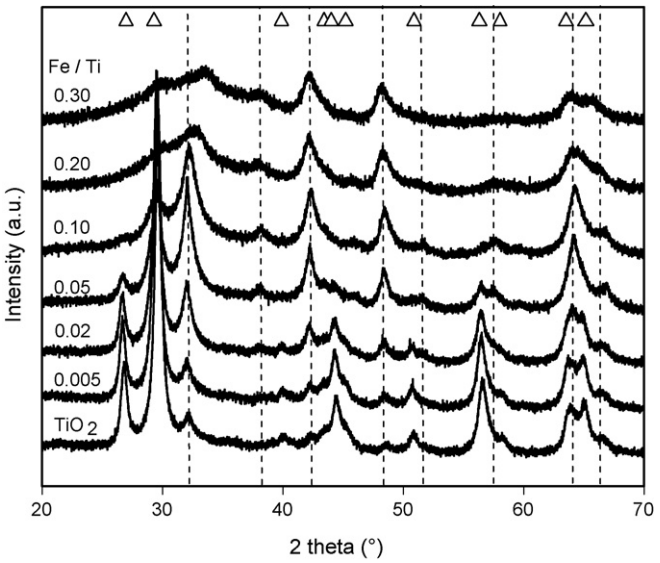

Fig. 4. X-ray diffraction pattern (Co Kα and Co Kβ radiation) of the FSP-made bare and Fe-doped TiO_2. The highly crystallined TiO_2 consists of predominantly anatase (△), but doping with Fe gradually enhances the transformation to rutile (- - -) and formation of amorphous content.

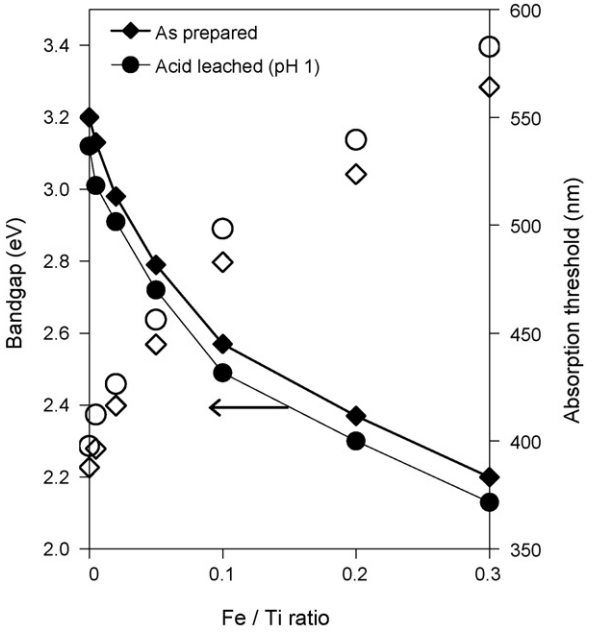

Fig. 3. Optical bandgap energy and its corresponding absorption threshold of bare and Fe-doped TiO_2 as-prepared and after leaching with 0.1N H_2SO_4 for 48 h, as function of metal loading.

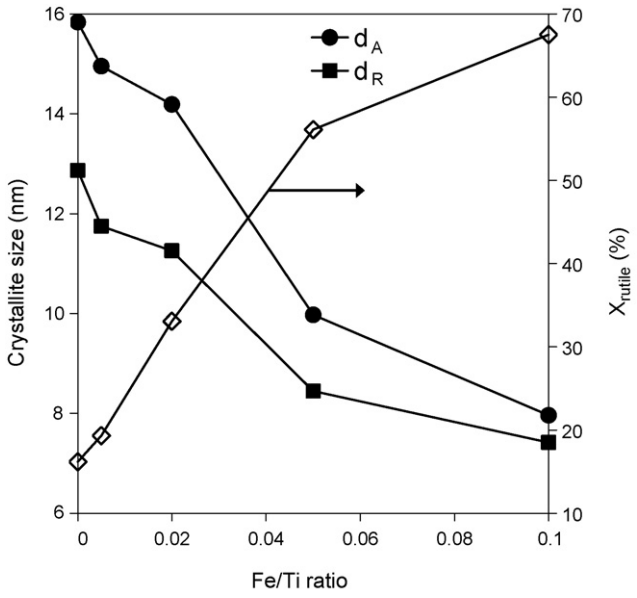

Fig. 5. XRD-determined anatase (d_A) and rutile (d_R) crystallite sizes and the corresponding rutile fraction of FSP-made bare and Fe-doped TiO_2 (Fe/Ti ≤ 0.1). The Cu Kα was used as the radiation source.

Ti^{4+} and creating oxygen vacancies that enhance the anatase to rutile transformation as observed here also. Wang et al. [45] claimed the smaller ionic radius of Fe^{3+} resulted in the compaction of TiO_2 lattice and hence the formation of a denser rutile phase (ρ_{rutile} = 4.26 g/cm^3 compared to $\rho_{anatase}$ = 3.84 g/cm^3). Besides, it has also been reported that calcination of Fe-impregnated TiO_2 could catalyse the transformation of anatase to rutile at above 550 °C [46]. Further, it can be seen from Fig. 5 that doping with Fe decreases both the anatase and rutile crystallite sizes.

As shown in the XRD spectra in Fig. 4, a gradual shift from the TiO_2 rutile (1 1 0) peak of $2\theta = 31.9^\circ$ was observed for Fe-doped TiO_2 with high Ti/Fe ratios of 0.10 (32.4°), 0.20 (33.0°) and 0.30 (33.6°) consistent with Al-doped TiO_2 [43]. The shifted peak did not match any of the Fe-based crystallite phases such as magnetite (Fe_3O_4, PDF:003-0862), maghemite (γ-Fe_2O_3, PDF:004-0755), hematite (α-Fe_2O_3, PDF:003-0800), psudobrookite (Fe_2TiO_5, PDF:009-0182), pseudorutile ($Fe_2Ti_3O_9$, PDF:013-0326), ilmenite ($FeTiO_3$, PDF:003-0781) to ulvospinel (Fe_2TiO_4, PDF:018-0658). The shift at high Fe-dopant content does not only coincide with the broad band observed in the UV–vis spectra (Fig. 2a) as described earlier, but is also accompanied by the formation of XRD amorphous band at $2\theta = 21–43^\circ$ (Fig. 4). The formation of an amorphous hump is consistent with other previously reported work at high Fe-dopant content [28,45]. It is believed that excessive Fe doping disturbs the arrangement of the TiO_2 basic octahedral units [47] and hence distorts the overall crystallite structure.

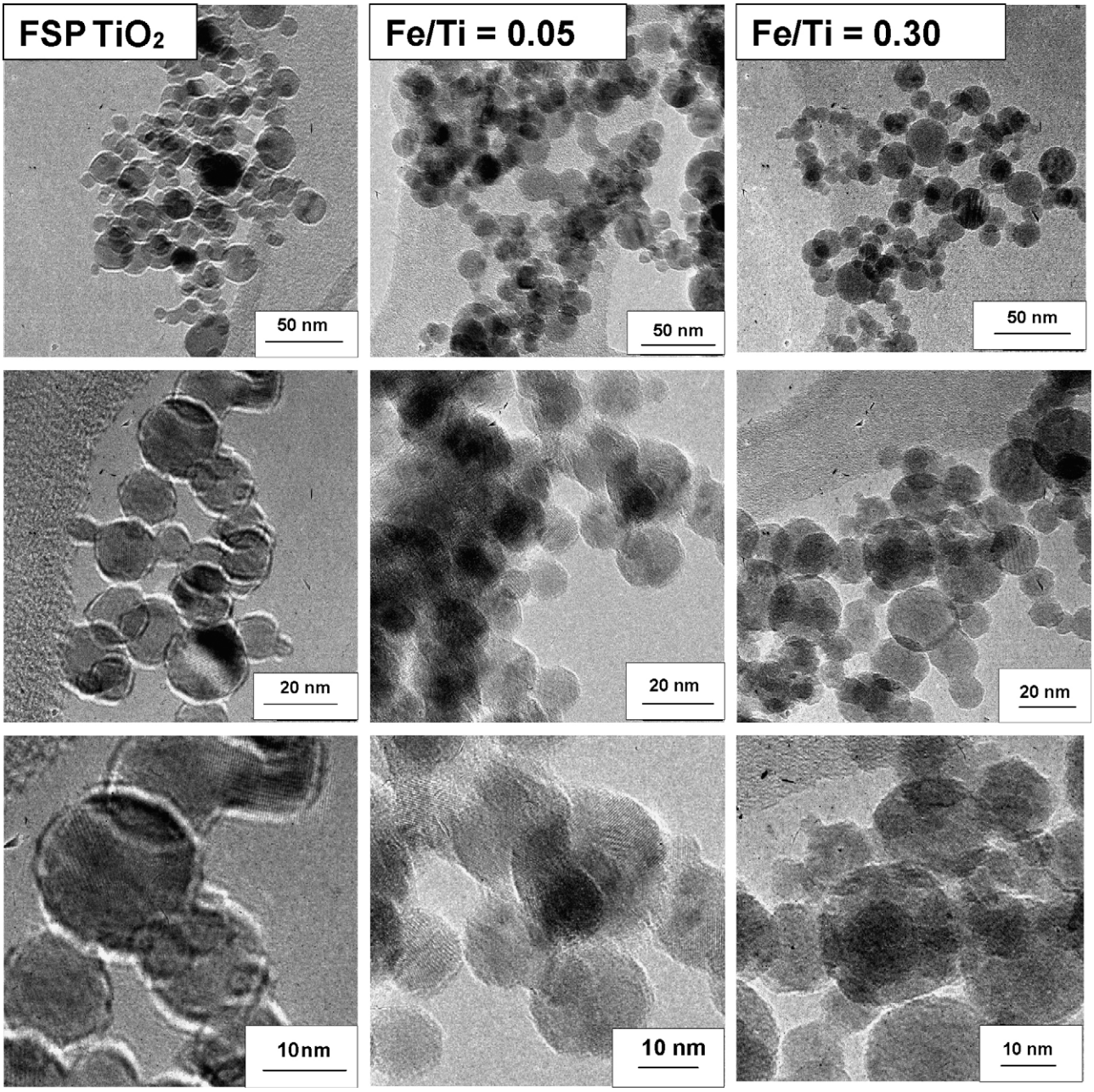

Fig. 6. TEM micrographs of FSP-made (a) TiO_2, (b) Fe/Ti = 0.05 and (c) 0.30 at different magnifications.

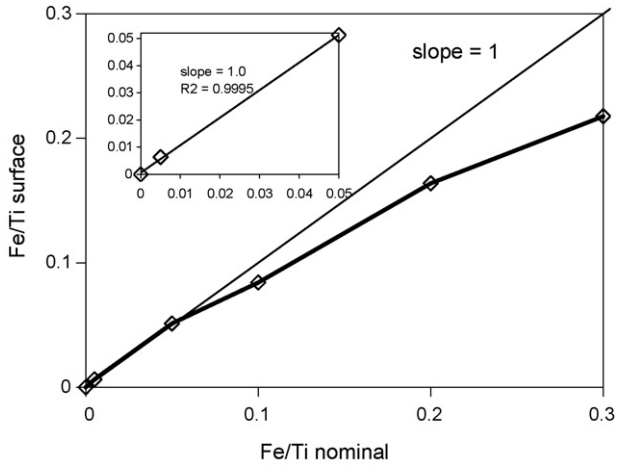

Fig. 7. The ratio of Fe/Ti measured by XPS on the surface of Fe-doped TiO_2 as a function of the nominal Fe/Ti loading. The inset shows the profile for Fe/Ti $\leq$ 0.05.

The amorphous phase is in excellent agreement with that observed under TEM (Fig. 6). Bare TiO_2 particles (Fig. 6a) with well-defined lattice fringes could be seen. By contrast, at Fe/Ti ratio of 0.05 (Fig. 6b), lattice fringes are still visible but less obvious than bare TiO_2 (Fig. 6a) indicating a limited extent of crystal modification. At Fe/Ti = 0.3 (Fig. 6c), mainly amorphous structures with very little lattice fringes could be seen.

Despite the consistency of various characterisation techniques as discussed above, the solubility limit of FSP-made Fe-TiO_2 remains rather ambiguous. Formation of a new Fe phase could not be detected from XRD even at high Fe/Ti ratio, presumably due to the well dispersed and small segregated Fe grains. Hence, an alternative and more sensitive XPS technique was employed. From Fig. 7 (inset), it is evident that there exists good agreement between nominal (bulk) Fe/Ti and XPS-determined surface Fe/Ti for ratios of $\leq$0.05, corroborating a homogeneous mixing at the atomic scale. As Fe loading is increased (Fe/Ti $\geq$ 0.10), the surface Fe/Ti becomes smaller than the nominal Fe/Ti, indicating phase segregation. Hence the solubility limit of Fe in TiO_2 is reached at an Fe/Ti ratio of approximately 0.05. Further doping of TiO_2 with Fe resulted in the appearance of an optical band centred at 490 nm, formation of amorphous structure, shift in rutile peak ($2\theta = 31.9^\circ$) and decrease in surface area (Fig. 8). As a comparison, the XRD spectra of the vapour-fed flame synthesised Fe-TiO_2 reported by Wang et al. [45] showed the formation of Fe phase at Fe/Ti ratio of 0.10. The conventional wet-preparation technique such as co-precipitation followed by high temperature calcination, however, gave much lower Fe solubility limit in TiO_2. Cordischi et al. [48] reported a solubility limit of around 1 at.% Fe (equivalent to Fe/Ti $\geq$ 0.01) in anatase but only ~0.1 at.% (Fe/Ti~ 0.001) in similarly prepared rutile but calcined at much higher temperature (>600 °C). Li et al. [26] also found a solubility limit of ~1 at.% Fe in anatase prepared by a sol–gel process followed by annealing at 450 °C for 2 h. Hence it can be deduced that the gas-to-particle FSP approach may give a higher Fe solubility limit in TiO_2 compared to that produced in conventional wet technique followed by high temperature calcinations. This is conceivably due to short residence time and high quenching rate of FSP. As shown in Table 1, the Fe oxidation state of the as-prepared photocatalysts exists predominantly of Fe(III), with the remaining being made up of Fe(II).

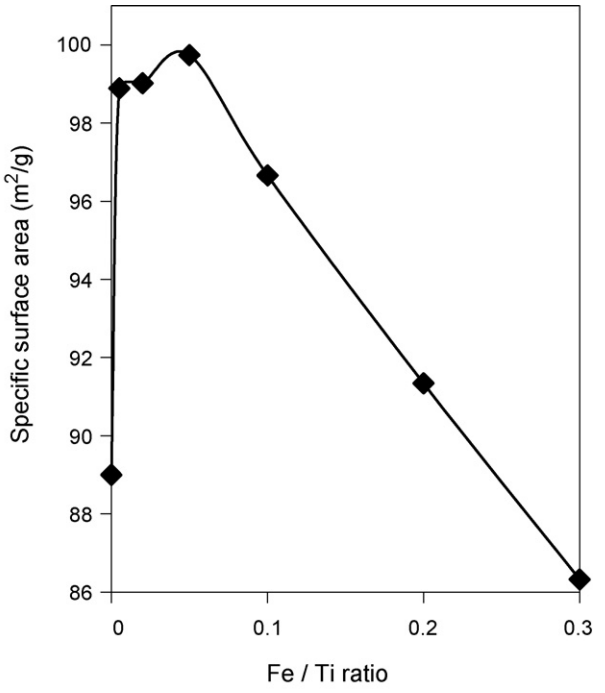

Fig. 8. Specific surface area of as-prepared pure and Fe-doped TiO_2 photocatalyst samples as a function of metal loading.

3.3. Photocatalytic mineralisation of oxalic acid

The dissociation constant of oxalic acid were previously reported as $pK_1 = 1.25$ and $pK_2 = 4.28$ [49]. Hence at the present experimental condition of pH 3.25 $\pm$ 0.25, more than 98% of the oxalic acid exists in its ionic form with at least 85% forming $HC_2O_4^-$. In the absence of photocatalyst and light source, neither mineralisation of the parent oxalic acid nor its dissociated ions could be detected, reconfirming the observation by Navío et al.

Table 1
Ratio of Fe/Ti and Fe(III)/Fe(total) on the surface of FSP-made bare TiO_2 and Fe-doped TiO_2 determined by XPS analysis before photocatalytic reactions

Fe/Ti ratio (nominal)	Reaction runs	Fe/Ti ratio (surface)	Fe(III)/Fe (total) (%)
0.000	0	0	0
0.005	0	0.006	100
0.050	0	0.051	91
0.100	0	0.084	93
0.200	0	0.164	100
0.300	0	0.218	100
0.050	1	0.051	86
0.050	5	0.036	82

Also shown are the Fe/Ti and Fe(III)/Fe(total) ratios (for the Fe-doped TiO_2 with nominal Fe/Ti ratio of 0.05) after 1 and 5 repeated runs of photocatalytic mineralisation of oxalic acid. Binding energy Fe(III) ~ 711.1 and 713.0 eV. Binding energy Fe(II) ~ 709.3 eV.

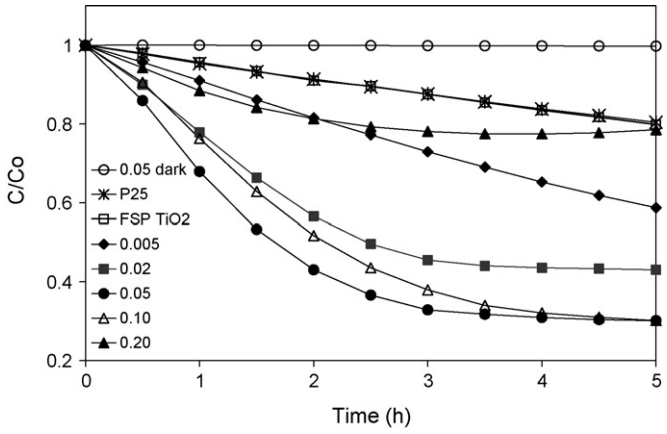

Fig. 9. Mineralisation of 10 ppm (as carbon) of oxalic acid by bare and Fe-doped TiO_2 under visible light irradiation ($\lambda > 400$ nm). The numbers in the legend represents the Fe/Ti ratio.

[40]. Under visible light irradiation ($\lambda > 400$ nm), relatively slow but comparable mineralisation kinetics could be observed for Degussa P25 and FSP-made TiO_2 (Fig. 9). This is not surprising considering the many similarities shared between the two photocatalysts as described earlier. In fact, it was recently found that the photocatalytic activity of both catalysts was similar in mineralising a range of carboxylic acids under near-UV illumination [35]. The observed mineralisation under visible light in this work for undoped TiO_2 is attributed to the excitation of rutile (absorption threshold ~414 nm). It is worth pointing out as well that despite inactivation of anatase (absorption threshold ~388 nm) under visible light, it does not rule out the possibility of photogenerated charge transfer between the two crystallite phases, hence allowing for photocatalytic reaction to take place on anatase surface [50].

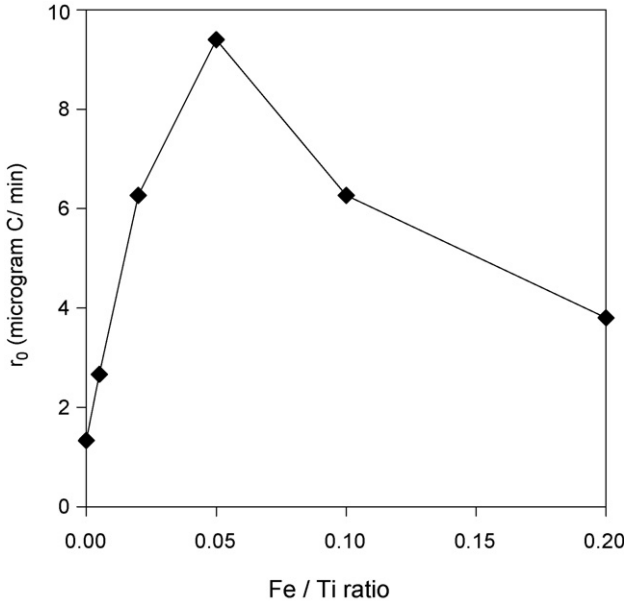

Fig. 10. Initial rates of photocatalytic mineralisation of 10 ppm (as carbon) of oxalic acid by bare and Fe-doped TiO_2 at different dopant levels. The initial rates were determined over the first half hour.

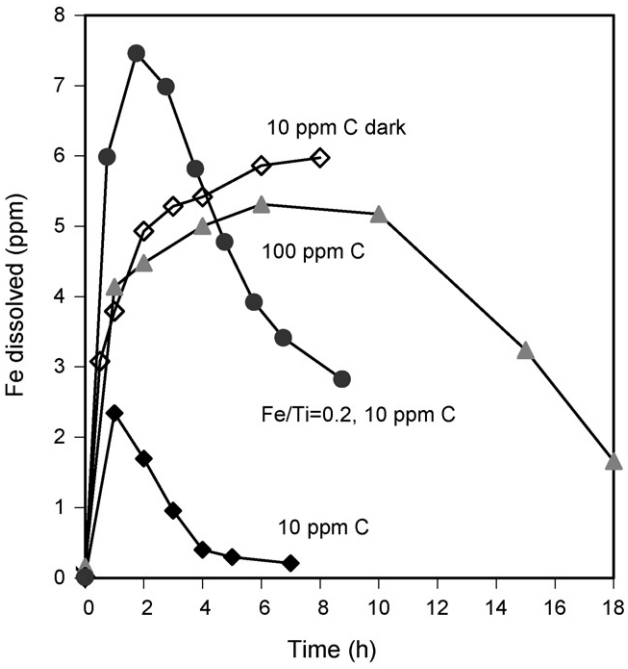

Fig. 11. Leaching dynamics of Fe by different concentrations of oxalic acid with and without visible light irradiation. Unless otherwise stated, the Fe-doped TiO_2 samples have Fe/Ti ratio of 0.05.

As shown in Figs. 9 and 10, doping TiO_2 with Fe for Fe/Ti ratio of up to 0.05 drastically improves the mineralisation of oxalic acid under visible light irradiation. No dark mineralisation could be observed even for the most active photocatalyst, i.e. for Fe/Ti ratio of 0.05, confirming the observed mineralisation of oxalic acid is mainly due to photoreaction. Although the dependencies of reaction rates on Fe loading coincides well with the specific surface area profile shown in Fig. 8, it is unlikely that the 6.4-fold improvement in photocatalytic activity is solely the result of the slight 1.12-fold increase in surface area. In order to gain more in-depth understandings on the photocatalytic activity enhancement, it is essential to inspect the role of Fe in the reaction. Fig. 11 reveals a unique initial Fe dissolution and re-adsorption at the end of oxalic acid mineralisation under visible light. Such behaviour was first reported by Araña et al. [51,52] during the degradation of formic, maleic and acetic acids under UV illumination by Fe-TiO_2 synthesised by impregnation and sol–gel synthesis. It is interesting to note from the current work that the unique leaching characteristic is extended to visible light irradiation. The amount of Fe(III) leached out during the photocatalytic reaction was found to be strongly dependent on Fe loading and the amount of oxalic acid in aqueous suspension (Fig. 11).

In order to extract Fe(III) from the photocatalyst surface, it is envisaged that oxalic acid would have to firstly adsorb onto the photocatalyst surface (Eq. (2)). The zeta potential dynamic studies on Fe-doped TiO_2 sample Fe/Ti = 0.05 revealed a strong negatively charged zeta potential of −22 mV upon addition of oxalic acid (see Fig. 12), compared to +18 mV for the same particle in the absence of oxalic acid. The shift to a negatively charged zeta potential has been previously reported to be caused by the adsorbed carboxylic acid [35,53]. Given the

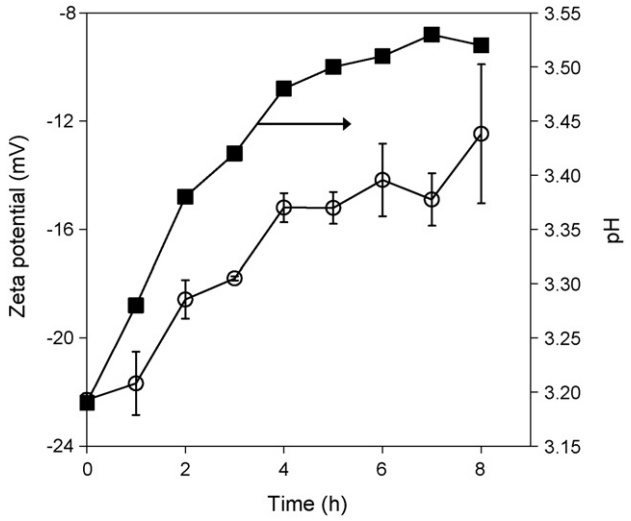

Fig. 12. Zeta potential dynamics of Fe-doped TiO_2 particles (Fe/Ti = 0.05) and the corresponding solution pH during photocatalytic mineralisation of 10 ppm (as carbon) of oxalic acid.

abundance of negatively charged dissociated oxalate ions and positively charged photocatalyst surface, the adsorbed species are most likely a mixture of $HC_2O_4^-$ and $C_2O_4^{2-}$.

The continuous Fe-leaching in the absence of illumination (Fig. 11) confirmed that adsorption and leaching of Fe(III) by oxalic acid do not require visible light irradiation. The following scheme shows the reaction that might occur in the dark and under illumination:

$$Fe(III)_{ads} + oxalic_{ads} \xrightarrow{dark} Fe(III)\text{-oxalate} \quad (2)$$

$$Fe(III)\text{-oxalate} \xrightarrow{240-475\,nm} Fe(II) + CO_2 \quad (3)$$

$$Fe\text{-}TiO_2 \xrightarrow{visible} Fe\text{-}TiO_2{}^*(e^- + h^+) \quad (4)$$

$$Fe(II)_{ads} + h^+ \xrightarrow{visible/Fe\text{-}TiO_2} Fe(III)_{ads} \quad (5)$$

$$Fe(II) + O_2 \rightarrow Fe(III) + O_2^{\bullet -} \quad (6)$$

$$Oxalic + h^+ \xrightarrow{photoKolbe} CO_2 \quad (7)$$

$$O_2 + e^- \xrightarrow{visible/Fe\text{-}TiO_2} O_2^{\bullet -} \quad (8)$$

Upon irradiation with visible light, the Fe(III)-oxalate complex is easily photolysed to CO_2 [54], presumably by photoinduced intrinsic charge transfer between Fe(III) and oxalate ions (Eq. (3)). This resulted in free Fe(II) which is unable to take part in subsequent reactions [52] without first being re-oxidised. However, the decreasing trend of Fe-leaching under illumination in comparison to the continuous Fe dark leaching (Fig. 10) implies that Fe(II) is quickly re-adsorbed back onto photocatalyst surface. The adsorbed Fe(II) is subsequently re-oxidised by visible light induced photo-generated holes (Eq. (4) and (5)) or dissolved O_2 (Eq. (6)) to form Fe(III) where it could then further take part in the photoreaction. This is a crucial step to ensure sustainability of Fe in the mineralisation of oxalic acid. However under the present experimental condition, regeneration of Fe(II) by dissolved O_2 (Eq. (6)) is somewhat less efficient than that by photogenerated holes, as will be discussed later in Section 3.4. Formation of H_2O_2 via photoexcitation of Fe(II) is also unlikely especially at acidic pH [55] hence ruling out the possibility of Fenton or photo-Fenton reactions. Analysis of the as-prepared and used Fe-TiO_2 by XPS revealed only a slight decrease (5%) of Fe(III) content in the latter after the first reaction run (Table 1). Despite repeating the reaction for 5 consecutive runs, only a further decrease of 4% Fe(III) could be detected (Table 1), implying that most Fe(II) were converted back to Fe(III) upon re-adsorption. It should be stressed here that in all cases, direct oxidation of oxalic acid to CO_2 by photogenerated holes (Eq. (7)) must not be ruled out. Nevertheless, it is rather difficult to distinguish between the direct hole oxidation and Fe(III)-mediated photoreaction. In fact, Quici et al. [33] also pointed out that the concurrent homogeneous process complicates the heterogeneous reactions. Additionally, the complex Fe dissolution and re-adsorption properties make differentiation between the two oxidation mechanisms difficult.

Excellent agreement between the trend of oxalic acid mineralisation and zeta potential can be seen from Figs. 9 and 12, respectively. Continuous oxalic acid mineralisation for the first 4 h of irradiation was well reflected in the progressive positive shift in zeta potential, indicating a decreasing amount of organic compounds. Likewise, as little CO_2 evolution was detected after 4 h, the particle zeta potential also remained constant indicating insignificant change in the amount of surface organics. Analysis of the filtered suspension after 5 h using the conventional total organic carbon (TOC) analyser did not detect any significant amount of carbon in the solution. A careful interpretation should be adopted here as total removal of carbon from aqueous phase does not mean total mineralisation of organic substrate. In fact the low carbon content in the aqueous could be simply due to the strong adsorption of oxalic acid or its intermediate products on the photocatalyst surface. This is possible considering their charge attractions and the high photocatalyst surface area. Although not shown here, irradiation with UVA lamp at the end of visible light illumination to burnoff remaining carbon on the photocatalyst surface revealed further CO_2 evolution and restored the photocatalyst zeta potential to its original value of +18 mV.

To further elucidate the interaction between dissolved Fe and the modified photocatalyst, Fe-leaching during oxalic acid mineralisation by Fe/Ti = 0.20 was also investigated. Fig. 11 showed that despite the higher amount of Fe dissolved when using this photocatalyst, it did not result in a similar increase in oxalic acid mineralisation rate. In fact, the mineralisation rate was lower than that of Fe/Ti = 0.05. This can be explained as due to excessive charge recombination and non-photoactive amorphous formation, thus lowering the efficiency of Fe(II) reoxidation. The same reasons could also be applied to explain the decreasing trend in photocatalytic activity of the other samples Fe-doped TiO_2 with Fe/Ti $\geq$ 0.1.

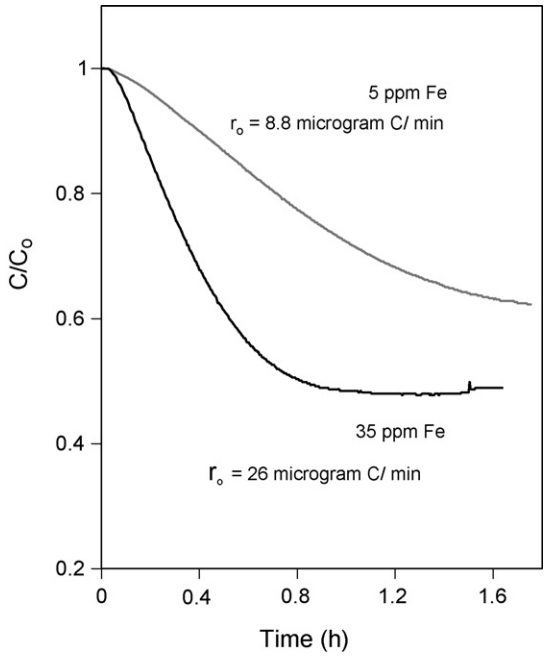

Fig. 13. Mineralisation of 10 ppm (as carbon) of oxalic acid by bare TiO_2 and dissolved Fe(III) as perchlorate under visible light irradiation ($\lambda > 400$ nm).

3.4. Oxalic acid mineralisation by dissolved Fe(III)/TiO_2

As a comparison with the Fe-doped TiO_2 sample, mineralisation of oxalic acid was carried out in the same way, but using 5 and 35 ppm Fe(III) in the form of $Fe(ClO_4)_3$ coupled with FSP-made bare TiO_2. The amount of 5 ppm Fe(III) is approximately the amount of Fe present on the photocatalyst surface with Fe/Ti ratio of 0.05, while the latter amount is equal to the Fe concentration if all the Fe on surface and bulk is leached out. As can be seen clearly in Fig. 12, the initial rate of oxalic acid mineralisation at high Fe concentration was much faster than that of Fe-doped samples. This is due to the efficient homogeneous reaction of dissolved Fe(III) and oxalic acid, compared to heterogeneous reactions, in overcoming mass transfer limitation. Previously reported work also found that addition of Fe(III) to TiO_2 suspension under UVA illumination drastically improves the initial rates of oxalic and maleic acids mineralisation [33,56].

However with only the presence of TiO_2, Fe(II) could not be regenerated efficiently even in the presence of dissolved O_2 (Eq. (5)), as all suspension was air-equilibrated prior to irradiation. This is evident in Fig. 13 in which the extent of photocatalytic mineralisation in the presence of dissolved Fe concentrations (40% and 50% for 5 and 35 ppm dissolved Fe, respectively) were lower than that of Fe-doped TiO_2 (70% mineralisation, Fe/Ti = 0.05). Moreover, since dissolved Fe(III) is unable to photosensitise TiO_2 [11], Fe(II) regeneration could only be carried out by the visible light inefficient TiO_2. The result in this work correlates well with the findings by Catastini et al. [55], who reported very slow Fe(II) reoxidation by dissolved O_2 (Eq. (5)) at pH 3 even in the presence of aeration and UV illumination (125 W).

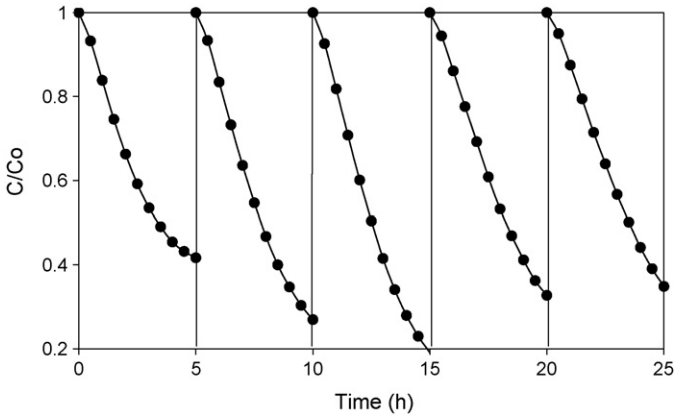

Fig. 14. Repeated mineralisation of 10 ppm (as carbon) of oxalic acid by Fe-doped TiO_2 (Fe/Ti = 0.05) under visible light irradiation ($\lambda > 400$ nm).

In terms of practical application, the addition of Fe(III) into the solution presents yet another great difficulty in recovering the dissolved Fe after the reaction and reusing the catalyst as will be demonstrated more clearly in the next section. The Fe-modified TiO_2 on the other hand has the unique capability of re-adsorbing most of the dissolved Fe at the end of reaction (Fig. 10).

3.5. Durability of Fe-doped TiO_2

To demonstrate the durability and reusability of the Fe-doped TiO_2, sample with Fe/Ti = 0.05 was subjected to repeated cycles of oxalic acid mineralisation under visible light. At the end of each run, the supernatant was replaced with fresh deionised water adjusted to pH 3.25 ± 0.25 with the aim of discarding any leached and non-adsorbed Fe ions. It can be seen from Figs. 14 and 15 that the rate of oxalic acid

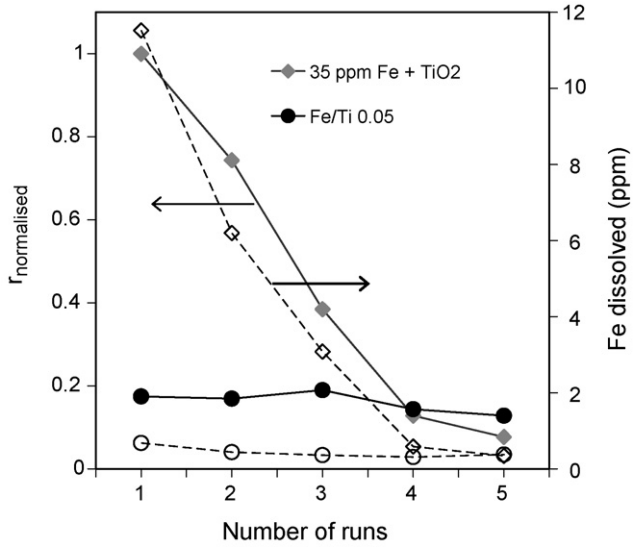

Fig. 15. Normalised initial rates of photocatalytic mineralisation of 10 ppm (as carbon) of oxalic acid (solid symbols) by Fe-doped TiO_2 (Fe/Ti = 0.05) and dissolved 35 ppm dissolved Fe(III) + TiO_2, and the corresponding loss of Fe (open symbols) at every repeated run. All initial rates were normalised with respect to the initial rate of the 35 ppm Fe(III) + TiO_2 in the first run.

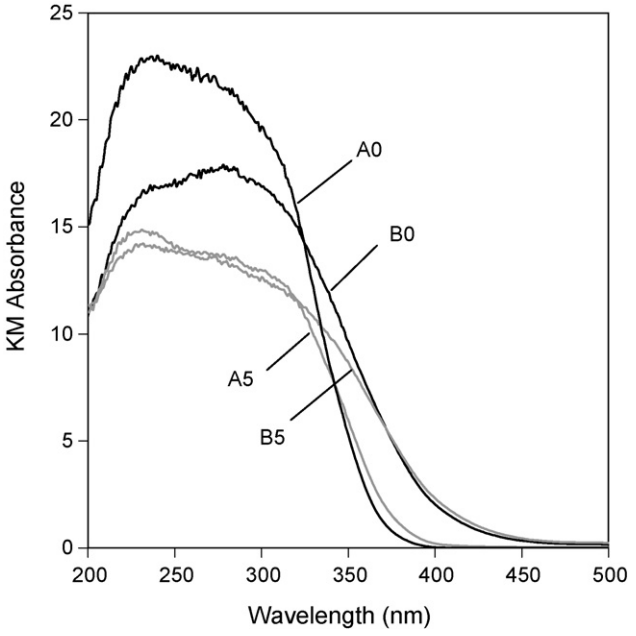

Fig. 16. Comparison of Kubelka–Munk absorption of as-prepared FSP TiO_2 (A0) and Fe-doped TiO_2 (Fe/Ti = 0.05) (B0) with the recovered 35 ppm Fe(III) + TiO_2 (A5) sample and Fe/Ti = 0.05 (B5), respectively, after 5 repeated runs of oxalic acid mineralisation.

mineralisation by Fe-doped TiO_2 remained fairly consistent throughout the 5 repeated runs. This can be attributed to the minimal Fe-leaching at the end of each run. Although the surface Fe/Ti ratio (Table 1) depleted from 0.051, for both the unused photocatalyst and the photocatalyst after 1 run, to 0.036 for the photocatalyst after 5 runs, it did not significantly affect mineralisation of oxalic acid. The Fe depletion is only restricted to that from the particle surface while the bulk photocatalyst remains visible light-active. Hence the photocatalytic activity was not significantly affected throughout the 5 repeated runs. Additionally, it can be seen from Fig. 9 that the sample with Fe/Ti = 0.02, which has only 40% of the bulk Fe concentration of the sample Fe/Ti = 0.05 still shows considerable activity. Further studies are needed to study the activity of the photocatalyst in longer runs. The mixture of 35 ppm dissolved Fe(III) and FSP-made bare TiO_2, on the other hand, shows deteriorating reaction rates after each run. The drastic deactivation can be attributed to the massive loss of unadsorbed Fe at the end of each run. As discussed earlier, pure TiO_2 has limited capability of re-adsorbing and re-generating Fe(II). Hence it is not surprising that on the fifth run, as 80% of the initial dissolved Fe has been leached out and removed from the suspension, the rate of reaction decreased by 90% and less active than the FSP-made Fe-TiO_2.

Fig. 16 shows the absorbance spectra of the recovered photocatalysts at the end of 5 repeated runs. The optical bandgap of sample Fe/Ti = 0.05 remains unaltered before and after the repeated runs. This gives concrete evidence that the bandgap of Fe-modified TiO_2 is photo and chemically stable even after repeated usage. On the other hand, addition of dissolved Fe(III) to pure TiO_2 did not significantly affect the bandgap of the photocatalyst. The slight red-shift observed in the used catalyst was likely due to adsorbed residue Fe. Franch et al. [56] also found chemisorbed Fe ions on TiO_2 surface carrying over to subsequent repeated run despite washing and partial drying after the first run. Unfortunately, no quantification of the remaining amount of chemisorbed Fe was reported after washing.

4. Conclusions

The use of a one-step FSP technique to synthesise visible light-active Fe-doped TiO_2 photocatalyst has been demonstrated. Introduction of Fe into TiO_2 matrix by flame synthesis was effective in extending the particle photoresponse to the visible regime ($\lambda > 400$ nm). At the same time, it also enhances transformation to rutile. Being a bottom-up approach, the short residence time coupled with a high quenching rate during the FSP process was found to be an excellent method in synthesising homogeneous Fe-doped TiO_2 solid solutions with high Fe solubility. The reported solubility of up to Fe/Ti = 0.05 in this work is significantly higher than the Fe/Ti $\sim$ 0.01 commonly found for particles synthesised by wet techniques followed by high temperature calcination. Doping Fe above its solubility limit was accompanied by formation of amorphous structure and a UV–vis optical band centred at 490 nm. A slight shift in the XRD rutile (1 1 0) peak and a decrease in specific surface area were also observed at high Fe loadings.

The Fe-TiO_2 sample was able to mineralise oxalic acid under visible light. This is also accompanied by a unique Fe-leaching and re-adsorption properties. Extraction of Fe(III) from photocatalyst surface was found to take place even in the dark to form an Fe(III)-oxalate complex. The complex is photolysed under visible light irradiation leaving behind Fe(II) ions. Here, the presence of visible light-active Fe-TiO_2 is important to re-oxidise the adsorbed Fe(II) to Fe(III) to sustain the photoreaction under visible light. A high extent of oxalic acid mineralisation (70%) for 10 ppm (as carbon) of oxalic acid was observed for Fe-doped TiO_2 with Fe/Ti ratio of 0.05 compared to just 50% for the same bulk amount of aqueous Fe(III) and TiO_2. In addition, most dissolved Fe ions are re-adsorbed back on the Fe-TiO_2 particles at the end of the oxalic acid oxidation reaction, thereby minimizing the loss of Fe and rendering its re-usability. On the other hand, a mixture of dissolved Fe(III) and bare TiO_2 resulted in significant loss of unadsorbed Fe after each run. Hence it is not surprising that the Fe-doped TiO_2 particles exhibited reproducible mineralisation rates even after 5 repeated runs whereas the latter saw deteriorating rates after every run. The UV–vis absorption spectrum of Fe-doped TiO_2 was also found to be unchanged despite repeated photocatalytic runs.

Acknowledgments

L. Mädler thanks the Parson's foundation for their support. This work was produced with the financial assistance of the Australian Research Council under the ARC Centres of Excellence Program.

References

[1] A. Fujishima, K. Honda, Nature 238 (1972) 37.
[2] B. Kraeutler, A.J. Bard, J. Am. Chem. Soc. 100 (1978) 2239.
[3] B. O'Regan, M. Grätzel, Nature 353 (1991) 737.
[4] R. Cai, Y. Kubota, T. Shuin, H. Sakai, K. Hashimoto, A. Fujishima, Cancer Res. 52 (1992) 2346.
[5] D.F. Ollis, H. Al-Ekabi (Eds.), Photocatalytic Purification and Treatment of Water and Air, Elsevier, Amsterdam, 1993.
[6] J. Yuan, S. Tsujikawa, J. Electrochem. Soc. 142 (10) (1995) 3444.
[7] R. Wang, K. Hashimoto, A. Fujishima, M. Chikuni, E. Kojima, A. Kitamura, M. Shimohigoshi, T. Watanabe, Nature 388 (1997) 431.
[8] H. Honda, A. Ishizaki, R. Soma, K. Hashimoto, A. Fujishima, J. Illum. Eng. Soc. Winter (1998) 42.
[9] K. Hara, H. Sugihara, Y. Tachibana, A. Islam, M. Yanagida, K. Sayama, H. Arakawa, G. Fujihashi, T. Horiguchi, T. Kinoshita, Langmuir 17 (2001) 5992.
[10] W. Choi, A. Termin, M.R. Hoffmann, J. Phys. Chem. 98 (1994) 13669.
[11] N. Serpone, D. Lawless, J. Disdier, J.-M. Herrmann, Langmuir 10 (1994) 643.
[12] E. Borgarello, J. Kiwi, M. Grätzel, E. Pelizetti, M. Visca, J. Am. Chem. Soc. 104 (1982) 2996.
[13] M. Anpo, Bull. Chem. Soc. Jpn. 77 (2004) 1427.
[14] M. Anpo, Catal. Surv. Jpn. 1 (1997) 169.
[15] H. Yamashita, M. Harada, J. Misaka, M. Takeuchi, B. Neppolian, M. Anpo, Catal. Today 84 (2003) 191.
[16] M. Matsuoka, M. Kitano, M. Takeuchi, M. Anpo, J.M. Thomas, Mater. Sci. Forum 486 (2005) 81.
[17] R. Asahi, T. Morikawa, T. Ohwaki, K. Aoki, Y. Taga, Science 293 (2001) 269.
[18] K. Kobayakawa, Y. Murakami, Y. Sato, J. Photochem. Photobiol. A: Chem. 170 (2005) 177.
[19] D. Li, H. Haneda, S. Hishita, N. Ohashi, Mater. Sci. Eng. B 117 (2005) 67.
[20] T. Ohno, T. Mitsui, M. Matsumura, Chem. Lett. 32 (4) (2003) 364.
[21] J.C. Yu, W. Ho, J. Yu, H. Yip, P.K. Wong, J. Zhao, Environ. Sci. Technol. 39 (2005) 1175.
[22] L. Gao, H. Liu, J. Sun, Mater. Sci. Forum 53 (2005) 486.
[23] C. Lettmann, K. Hildenbrand, H. Kisch, W. Macyk, W.F. Maier, Appl. Catal. B: Environ. 32 (2001) 215.
[24] S.U.M. Khan, M. Al-Shahry, W.B. Ingler Jr., Science 297 (2002) 2243.
[25] S. Sakthivel, H. Kisch, Angew. Chem. Int. Ed. 42 (2003) 4908.
[26] X. Li, P.-L. Yue, C. Kutal, New J. Chem. 27 (2003) 1264.
[27] K. Nagaveni, M.S. Hegde, G. Madras, J. Phys. Chem. B 108 (2004) 20204.
[28] F. Gracia, J.P. Holgado, A. Caballero, A.R. Gonzales-Elipe, J. Phys. Chem. B 108 (2004) 17466.
[29] E.P. Reddy, B. Sun, P.G. Smirniotis, J. Phys. Chem. B 108 (2004) 17198.
[30] M. Sokolowski, A. Sokolowska, A. Michalski, B. Gokieli, J. Aerosol Sci. 8 (1977) 219.
[31] L. Mädler, H.K. Kammler, R. Mueller, S.E. Pratsinis, J. Aerosol Sci. 33 (2002) 369.
[32] M.M. Kosanic, J. Photochem. Photobiol. A: Chem. 119 (1998) 119.
[33] N. Quici, M.E. Morgada, G. Piperata, P. Babay, R.T. Gettar, M.I. Litter, Catal. Today 101 (2005) 253.
[34] W.Y. Teoh, L. Mädler, D. Beydoun, S.E. Pratsinis, R. Amal, Chem. Eng. Sci. 60 (2005) 5852.
[35] W.Y. Teoh, F. Denny, R. Amal, D. Friedmann, L. Mädler, S.E. Pratsinis, Top. Catal., in press.
[36] J. Tauc, R. Grigorovici, A. Vanuc, Phys. Stat. Sol. 15 (1966) 627.
[37] R.A. Spurr, H. Myers, Anal. Chem. 29 (1957) 760.
[38] M. Abdullah, G.K.-C. Low, R.W. Matthews, J. Phys. Chem. 94 (1990) 6820.
[39] T. Umebayashi, T. Yamaki, H. Itoh, K. Asai, J. Phys. Chem. Solids 63 (2002) 1909.
[40] J.A. Navío, G. Colón, M.I. Litter, G.N. Bianco, J. Mol. Catal. A: Chem. 106 (1996) 267.
[41] R.D. Shannon, Acta Cryst. A32 (1976) 751.
[42] M.C. Heine, L. Mädler, R. Jossen, S.E. Pratsinis, Combust. Flame 144 (4) (2006) 809.
[43] M.K. Akhtar, S.E. Pratsinis, S.V.R. Mastrangelo, J. Mater. Res. 9 (1994) 1241.
[44] S. Vemury, S.E. Pratsinis, J. Am. Ceram. Soc. 78 (1995) 2984.
[45] Z.-M. Wang, G. Yang, P. Biswas, W. Bresser, P. Boolchand, Powder Technol. 114 (2001) 197.
[46] L. Palmisano, M. Schiavello, A. Sclafani, C. Martin, I. Martin, V. Rives, Catal. Lett. 24 (1994) 203.
[47] X. Bokhimi, A. Morales, M. Aguilar, J.A. Toledo-Antonio, F. Pedraza, Int. J. Hydrogen Energy 26 (2001) 1279.
[48] D. Cordischi, N. Burriesci, F. D'Alba, M. Petrera, G. Polizzoti, M. Schiavello, J. Solid State Chem. 56 (1985) 182.
[49] Z.D. Draganic, M.M. Kosanić, M.T. Nenadović, J. Phys. Chem. 71 (1967) 2390.
[50] D.C. Hurum, A.G. Agrios, K.A. Gray, T. Rajh, M.C. Thurnauer, J. Phys. Chem. B 107 (2003) 4545.
[51] J. Araña, O. González Díaz, M. Miranda Saracho, J.M. Doña Rodríguez, J.A. Herrera Melián, J. Pérez Peña, Appl. Catal. B: Environ. 32 (2001) 49.
[52] J. Araña, O. González Díaz, M.J.M. Doña Rodríguez, J.A. Herrera Melián, C. Garriga I Cabo, J. Pérez Peña, M. Carmen Hidalgo, J.A. Navío-Santos, J. Mol. Catal. A: Chem. 197 (2003) 157.
[53] S.W. Lam, K. Chiang, T.M. Lim, R. Amal, G.K.-C. Low, in: Proceedings of the CHEMECA 2005, Brisbane, September 25–28, 2005.
[54] M.I. Litter, J.A. Navío, J. Photochem. Photobiol. A: Chem. 98 (1996) 171.
[55] C. Catastini, M. Sarakha, G. Mailhot, M. Bolte, Sci. Total Environ. 298 (2002) 219.
[56] M.I. Franch, J.A. Ayllón, J. Peral, X. Domènech, Catal. Today 101 (2005) 245.